applied sciences

MDPI

Article

Enhanced Neural Real-Time Digital Twin for Electrical Drives

Marco di Benedetto [1,*], Vincenzo Randazzo [2,*], Alessandro Lidozzi [1,3], Angelo Accetta [3,4], Giorgia Ghione [2], Luca Solero [1,3], Giansalvo Cirrincione [5] and Eros Gian Alessandro Pasero [2]

1 Department of Industrial, Electronic and Mechanical Engineering, Roma Tre University, 00146 Rome, Italy; luca.solero@uniroma3.it (L.S.)
2 Department of Electronics and Telecommunication (DET), Politecnico di Torino, 10129 Turin, Italy; giorgia.ghione@polito.it (G.G.); eros.pasero@polito.it (E.G.A.P.)
3 Department of Civil, Computer and Aeronautical Technologies Engineering, Roma Tre University, 00146 Rome, Italy; angelo.accetta@cnr.it
4 Institute of Marine Engineering (INM), Section of Palermo, National Research Council of Italy (CNR), 90146 Palermo, Italy
5 Laboratory LTI, University of Picardie Jules Verne, 80025 Amiens, France; nimzoexin59@gmail.com
* Correspondence: marco.dibenedetto@uniroma3.it (M.d.B.); vincenzo.randazzo@polito.it (V.R.)

Featured Application

The proposed neural real-time digital twin can be applied to offshore wind energy conversion systems for online condition monitoring and predictive maintenance of PMSG-based generators and power converters. By enabling sensorless estimation of degradation-sensitive parameters such as stator resistance, synchronous inductance, and DC-link capacitance, the method supports early fault detection, reduced downtime, and improved system reliability. The embedded implementation also makes it suitable for integration into industrial drive controllers and renewable energy platforms.

Abstract

This paper presents a real-time digital twin (DT) of the power conversion system used in offshore wind applications. The proposed DT is exploited to identify key electrical parameters of both the permanent magnet synchronous generator (PMSG) and the three-phase boost rectifier and has been developed with a Condition Monitoring (CM)-oriented approach. A Gated Recurrent Unit (GRU) neural network is adopted as a real-time digital model (RTDM) to estimate online the PMSG phase resistance and synchronous inductance, as well as the DC-link capacitance at the rectifier output. The network is trained in MATLAB using data generated by a Typhoon HIL 606 emulator, covering both balanced and unbalanced operating conditions and a wide range of parameter variations. The trained GRU is then deployed on the control board and implemented in LabVIEW Real-Time for embedded execution. Experimental tests on a PMSG-based generating unit confirm the effectiveness of the proposed RTDM, achieving low root-mean-square and mean percentage errors in parameter estimation. The results demonstrate that the enhanced neural real-time DT is a promising tool for condition monitoring and predictive maintenance of power conversion systems in offshore wind applications.

Keywords: digital twin; GRU; ordinary differential equations; power electronic converters

Academic Editor: Samuel Okegbile

Received: 2 March 2026
Revised: 3 April 2026
Accepted: 15 April 2026
Published: 18 April 2026

1. Introduction

The energy conversion sector has played a pivotal role in the global energy transition, particularly through renewable energy systems and electric vehicle charging stations,

where power electronic converters (PECs) have become the industry standard. Despite their critical importance, power conversion systems are among the most failure-prone assets in industrial environments [1,2]. Their susceptibility to operational and environmental stresses over time leads to gradual degradation and eventual failure [3,4]. After surviving the initial break-in period, the failure rate typically stabilizes at an approximately constant level until the PEC begins to wear out. However, unexpected overloads may occur during this period and are the main causes of random failures. In contrast, the primary causes of long-term failures are repeated thermal stresses followed by mechanical vibrations, which can cause components to reach the end of their lifetime before the product's expected service life. Critical parts such as power semiconductors, capacitors, electromechanical devices, and magnetic components therefore require robust design and testing to minimize failures [5]. Additionally, real-time monitoring of these components can help predict potential failures and improve long-term reliability. In this context, the concept of condition monitoring (CM) has emerged. CM in power electronics refers to the continuous assessment of the health and performance of components and systems to detect signs of degradation, wear, or impending failure. In general, CM methods can be divided into direct and indirect approaches [6]. Direct CM relies on physical sensors in direct contact with the system or component being monitored. For power modules, CM techniques are mainly classified into forward-voltage-based [7,8], threshold-voltage-based [9], switching-time-based [10], and temperature-based [11]. For capacitors, additional current or voltage sensors are usually required [12,13]. However, sensor-based CM increases both the cost and complexity of the system due to the additional hardware, which can itself reduce overall reliability. Moreover, most existing CM circuits and sensors are designed for specific components and cannot be easily generalized, limiting the applicability of these methods. Furthermore, degradation of a single power device or component affects the response of the entire power conversion system and, in practical maintenance strategies, a failure in one component often leads to replacement of the entire converter or assembly. Therefore, monitoring the health status of the entire power conversion system is crucial. This goal can be addressed through system identification techniques [14]. Parameter identification can be performed indirectly using algorithms such as recursive least squares [15] or Kalman filter [16]. However, when the number of unknown parameters exceeds the number of available equations, these algorithms may fail to provide feasible solutions. This limitation has motivated the recent adoption of the digital twin (DT) concept in the modelling and reliability assessment of power conversion systems. A DT is a high-fidelity digital replica of a particular power system (PS), capable of real-time online monitoring of the health status of one or more components by exploiting data from sensors already present in the PS and processing them using advanced optimization algorithms [17]. In recent years, numerous studies on DTs for estimating degradation parameters in power electronics have been published, employing a wide range of optimization algorithms [18–22]. However, metaheuristic optimization algorithms are iterative in nature, which makes parameter estimation time-consuming and, as the number of unknown parameters increases, the identification accuracy tends to deteriorate. For this reason, neural networks (NNs) are emerging as a promising solution for parameter estimation in power conversion systems.

The DT of a three-phase AC–DC boost rectifier was implemented in [23] to estimate the RL line impedance using NNs. In [24], the capacitance of a DC-link capacitor in a back-to-back converter was estimated using an artificial neural network (ANN) architecture that takes as inputs only the RMS value of the input current and the voltage ripple of the DC-link voltage. The identification of all the parameters of a buck converter was achieved in [25], where time- and frequency-domain features were extracted from current and voltage signals to train a backpropagation (BP) ANN. Despite the promising results reported in [25],

validation based solely on simulation data is not sufficient to fully validate an NN-based method. Experimental validation was presented in [26] for the identification of the on-state resistance of a MOSFET and the capacitance and equivalent series resistance of the output capacitor in a DC–DC buck converter. In particular, the proposed ANN method consists of two networks: ANN1, used to identify the MOSFET on-state resistance, and ANN2, used to estimate the capacitor capacitance and series resistance, thereby reducing the overall parameter estimation error. In [27], a monitoring method for degradation parameters of a DC–DC boost converter was developed using an NN and compared with a particle swarm optimization (PSO)-based health monitoring technique, demonstrating improved relative accuracy in parameter estimation. In [28], an ANN technique for estimating the parameters of a three-phase voltage source converter (VSC) has been implemented using as inputs the harmonics of the currents and voltage waveforms. Similarly to [27], also in [28] an ANN technique was implemented to estimate the parameters of a three-phase voltage source converter (VSC) using as inputs the harmonics of the current and voltage waveforms. Similarly to [27] the parameters estimated with ANN in [28] were compared to those obtained with a PSO algorithm, showing a reduction in the percentage error of about 10%.

NNs have also been applied to parameter estimation in electrical drives. In [29], an approach for online estimation of stator and rotor resistances in induction motors was proposed, enabling sensorless speed control in indirect vector-controlled drives using ANNs. Likewise, ref. [30] describes the hardware implementation of an NN-based estimator for the speed of the load machine in a drive system with elastic coupling, using a reconfigurable field-programmable gate array (FPGA).

Although these NN-based approaches demonstrate promising parameter estimation capabilities, they are typically designed as standalone estimators that map measured signals to unknown parameters. In most cases, the neural network is not structured as a real-time digital replica of the physical system, but rather as a regression tool operating independently from a digital representation of the converter or drive. Consequently, these methods do not fully exploit the digital twin paradigm, which requires a synchronized virtual model continuously updated using real-time measurements. To further clarify the distinction between conventional NN-based parameter estimation methods and the proposed approach, Table 1 summarizes the main differences between the two frameworks.

Table 1. Comparison between conventional NN-based parameter estimators and the proposed neural real-time digital twin.

Feature	Conventional NN/GRU Parameter Estimation	Proposed Neural Real-Time Digital Twin
Purpose	Parameter estimation	Real-time digital replica for condition monitoring
System representation	Single component or reduced model	Complete PMSG + rectifier system
Estimated parameters	Usually one or few parameters	Multiple parameters (Rs, Ls, Cdc) simultaneously
Digital twin paradigm	Not explicitly implemented	Explicit real-time digital twin
Operation mode	Offline or supervisory online estimation	Continuous real-time execution
Synchronization with plant	Not required	Synchronized with physical system
Embedded implementation	Often simulation or offline validation	Deployed on embedded controller
Real-time capability	Limited or not demonstrated	Demonstrated real-time execution

Table 1. *Cont.*

Feature	Conventional NN/GRU Parameter Estimation	Proposed Neural Real-Time Digital Twin
Condition monitoring capability	Indirect	Explicitly designed for CM
Sensor requirements	May require additional signals	Uses only existing measurements
Application scope	Converter or drive parameter estimation	System-level health monitoring

In this work, a neural real-time digital twin is defined as a data-driven digital replica of the power conversion system that operates synchronously with the physical plant and continuously updates its internal parameters using measured signals available in the controller. Unlike conventional NN-based parameter estimation methods, the proposed neural digital twin:

(i) Represents the complete PMSG rectifier system rather than a single component;
(ii) Performs simultaneous estimation of multiple degradation-sensitive parameters belonging to both the electrical drive and the power converter;
(iii) Operates in real time within the embedded controller;
(iv) Designed for condition monitoring purposes, enabling continuous tracking of parameter evolution during operation.

This formulation moves beyond conventional NN-based estimators by embedding the neural model within a real-time digital twin framework, where the GRU network acts as a real-time digital model (RTDM) of the system. The neural digital twin is therefore capable of providing continuous parameter updates, supporting health monitoring and predictive maintenance without requiring additional sensors or intrusive excitation signals. Although neural network–based parameter estimation methods reported in the literature show promising results, they are typically implemented as standalone regression tools that map measured signals to unknown parameters. In most cases, the neural model is not structured as a real-time digital replica of the physical system and does not operate synchronously with the plant. In contrast, the proposed approach embeds the GRU network within a neural real-time digital twin framework. The model represents the complete PMSG rectifier system and simultaneously estimates multiple degradation sensitive parameters, including stator resistance, synchronous inductance, and DC-link capacitance. Moreover, the digital twin operates in real time on the embedded controller using only measurements already available within the system, making it suitable for condition-monitoring applications. These features distinguish the proposed method from conventional neural network–based parameter estimation approaches.

Despite these advances, no prior work has demonstrated a NN-based digital twin that is simultaneously real-time, embedded, system-level, and experimentally validated under both balanced/unbalanced conditions and temperature variations for PMSG-based offshore wind power conversion systems.

The main contributions of the paper are the following:

- A neural real-time digital twin based on a GRU network is proposed for PMSG-based power conversion systems.
- Online estimation of stator resistance, synchronous inductance, and DC-link capacitance is achieved without additional sensors.
- The method is validated under wide parameter variations, balanced/unbalanced conditions, and different operating temperatures.

- The GRU model is deployed on an embedded controller using LabVIEW Real-Time, enabling true real-time execution.
- Experimental results demonstrate low RMSE and MPE, confirming suitability for condition monitoring and predictive maintenance in offshore wind applications.

2. PMSG and Converter Models

Figure 1 shows the power conversion system considered in this paper, where a three-phase boost converter is connected between the permanent magnet synchronous generator (PMSG) and the DC-link.

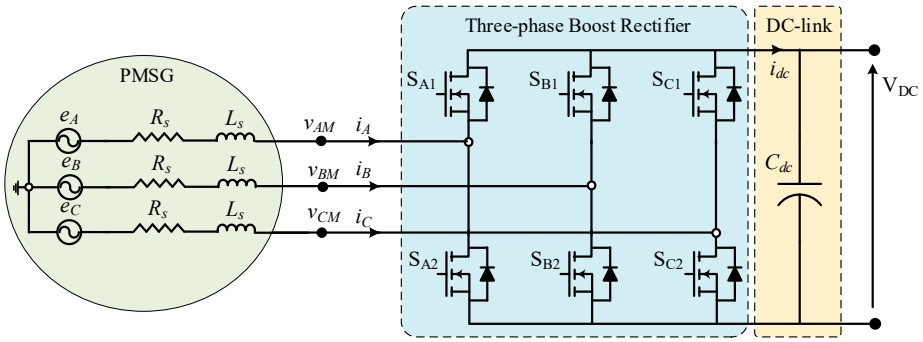

Figure 1. Electrical circuit model of the PMSG and three-phase boost rectifier.

2.1. Equivalent Model of the PSMG

Figure 2a shows the equivalent model of the PMSG, where R_s is the stator phase resistance, and λ_x is the permanent-magnet flux linkages, with $x \in \{A, B, C\}$. The mathematical model of the PMSG in the ABC reference frame can be expressed as in (1) and (2), where L_s is the synchronous inductance, and e_x are the three-phase back-EMF voltages.

$$\begin{cases} v_{AM}(t) = R_s i_A(t) + \frac{d\lambda_A}{dt} \\ v_{BM}(t) = R_s i_B(t) + \frac{d\lambda_B}{dt} \\ v_{CM}(t) = R_s i_C(t) + \frac{d\lambda_C}{dt} \end{cases} \tag{1}$$

$$\begin{cases} v_{AM}(t) = R_s i_A(t) + L_s \frac{di_A}{dt} + e_A \\ v_{BM}(t) = R_s i_B(t) + L_s \frac{di_B}{dt} + e_B \\ v_{CM}(t) = R_s i_C(t) + L_s \frac{di_C}{dt} + e_C \end{cases} \quad \begin{cases} v_d = R_s i_d + L_d \frac{di_d}{dt} - \omega_e L_q i_q \\ v_q = R_s i_q + L_q \frac{di_q}{dt} + \omega_e L_d i_d + \omega_e \lambda_{pm} \end{cases} \tag{2}$$

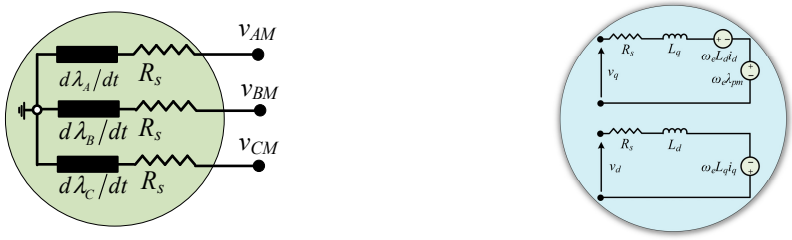

(**a**) (**b**)

Figure 2. Equivalent model of the PMSG from ABC (**a**) to dq reference frames (**b**).

Figure 2b depicts the equivalent model of the PMSG in the $dq0$ reference frame, rotating at synchronous frequency and whose direct axis is colinear with the PM axis. The corresponding mathematical model is written in (2), where v_d and v_q are the direct and quadrature axis components of the voltage space vector, L_d and L_q are the dq-axis inductances, i_d and i_q are the current space vector components along the $dq0$ axes. The

electromagnetic torque T_{em} of the machine can be expressed as in (3), where P is the number of pole pairs.

$$T_{em} = \frac{3}{2}P\left[\lambda_{pm}i_q + \left(L_d - L_q\right)i_d i_q\right] \tag{3}$$

To highlight the two different torque components, two coefficients K_{te} and K_{ta}, can be defined, shown in (5). K_{te} refers to the torque component due to the permanent magnets, whereas K_{ta} refers to the reluctance (anisotropy) torque component.

$$K_{te} = \frac{3}{2}P\lambda_{pm},\ K_{ta} = \frac{3}{2}P\left(L_d - L_q\right) \tag{4}$$

As a result, the electromagnetic torque of the machine can be written as in (5).

$$T_{em} = K_{te}i_q + K_{ta}i_d i_q \tag{5}$$

Furthermore, by applying Newton's second law, the mechanical equation of an electrical machine is given in (6), where T_L is the load torque, B is the viscous friction coefficient, and J is the moment of inertia of the rotating masses referred to the machine shaft.

$$\mathrm{J}\frac{d\omega_m}{dt} = T_L - T_{em} - \mathrm{B}\omega_m \tag{6}$$

The proposed model has been implemented for a Surface-Mounted PMSM (SM-PMSM). Owing to the choice of an SM-PMSM, the machine equations are further simplified, since the inductances have the same value on both the d and q axes and will be denoted by L_s from now on. Consequently, the torque constant K_{ta} is zero. The torque constant K_{te} is a known constant for a given electrical machine, as it depends only on the machine parameters P and λ_{pm}. Under these conditions, the machine torque depends only on the i_q current component, which is perpendicular to the magnetic flux. Therefore, since no flux weakening is needed, to obtain the maximum available torque, the i_d current component must be set to zero.

2.2. Equivalent Model of the System

Figure 3 shows the equivalent circuit model of the power conversion system in the ABC reference frame. Its mathematical description is given in (7), where V_{xM}, with $x \in \{A, B, C\}$, is the phase voltage provided by the converter, and V_{MN} is the middle (neutral) point voltage. The voltage V_{xM} depends on the switching function s_x as shown in (8).

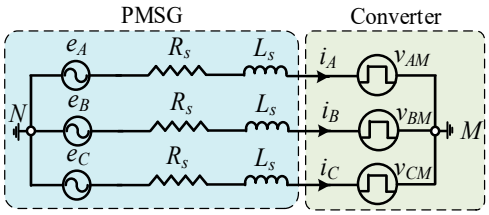

Figure 3. Equivalent circuit of the conversion system.

Assuming a symmetrical and balanced three-phase system, the midpoint voltage can be obtained as in (9). Substituting (9) into (7), the AC-side state-space model of the conversion system is obtained as in (10). Applying Kirchhoff's laws to the DC-side nodes of the circuit directly yields the equations reported in (11). The resulting combined set of

equations for the machine and converter model is given in (12), where m_d and m_q are the modulating signals in the $dq0$ reference frame.

$$\begin{cases} v_{AM} - V_{MN} = e_A - R_s i_A - L_s \frac{di_A}{dt} \\ v_{BM} - V_{MN} = e_B - R_s i_B - L_s \frac{di_B}{dt} \\ v_{CM} - V_{MN} = e_C - R_s i_C - L_s \frac{di_C}{dt} \end{cases} \tag{7}$$

$$\begin{cases} v_{AM} = V_{dc} s_A \\ v_{BM} = V_{dc} s_B \\ v_{CM} = V_{dc} s_C \end{cases} \quad \text{with } s_x = \begin{cases} 1 \\ 0 \end{cases} \tag{8}$$

$$V_{MN} = \frac{1}{2}(v_{AM} + v_{BM} + v_{CM}) \tag{9}$$

$$\begin{cases} L_s \frac{di_A}{dt} = e_A - R_s i_A - \frac{2}{3} v_{AM} + \frac{1}{3}(v_{BM} + v_{CM}) \\ L_s \frac{di_B}{dt} = e_B - R_s i_B - \frac{2}{3} v_{BM} + \frac{1}{3}(v_{AM} + v_{CM}) \\ L_s \frac{di_C}{dt} = e_C - R_s i_C - \frac{2}{3} v_{CM} + \frac{1}{3}(v_{AM} + v_{BM}) \end{cases} \tag{10}$$

$$C_{dc} \frac{dV_{dc}}{dt} = s_A i_A + s_B i_B + s_C i_C - i_{Load} \tag{11}$$

$$\begin{cases} L_s \frac{di_d}{dt} = \frac{V_{dc}}{2} m_d + P \omega_m L_s i_q - R_s i_d \\ L_s \frac{di_q}{dt} = \frac{V_{dc}}{2} m_q - P \omega_m \left(L_s i_d + \lambda_{pm} \right) - R_s i_q \\ C_{dc} \frac{dV_{dc}}{dt} = \frac{3}{4}\left(m_q i_q + m_d i_d \right) - i_{Load} \end{cases} \tag{12}$$

3. Parameters Identification Using Neural Networks

A type of neural network specialized for processing grid-like data, such as images, is the Convolutional Neural Network (CNN). CNNs use convolutional layers to extract features from the input data, making them particularly powerful for computer vision tasks such as image classification and object detection [31]. Recurrent Neural Networks (RNNs), on the other hand, are more effective for dynamic, time-dependent processes [32]. They are specifically designed for sequential data, such as time series or text. RNNs include recurrent connections that form cycles, allowing them to retain information over time. In particular, they can be configured to allow bidirectional information flow. In other words, while in Feed-Forward Neural Networks (FFNNs) the propagation of signals occurs only in the forward direction, from the inputs to the outputs, in RNNs this propagation can also occur from a subsequent layer to a previous one, between neurons within the same layer, or even from a neuron back to itself [33,34]. The most well-known variants of RNNs are Long Short-Term Memory (LSTM) networks and Gated Recurrent Units (GRUs), which address issues such as vanishing gradients and improve long-term memory retention. As mentioned previously, the NN selected in this work is the GRU. A GRU-based NN is a type of RNN that has gained popularity due to its relatively simple architecture. It is a recurrent network that uses the output values at a given time step as inputs for the next one, thus creating feedback and a correlation between past and future values, as shown in Figure 4.

As illustrated in the figure, the GRU NN is composed of: a reset gate r_t, which determines how much of the previous hidden state h_{t-1} to forget; an update gate z_t, which decides how much of the new candidate activation $\tilde{h}_t$ will be used to update the hidden state h_t; the candidate activation $\tilde{h}_t$, representing the potential new hidden state and incorporating the influence of the reset gate; and the actual hidden state h_t, which is a combination of the hidden state at the previous time step h_{t-1} and the candidate activation. The defining equations are given in (13), where σ is the sigmoid activation function, tanh is the hyperbolic tangent, W_{xr}, W_{xz}, and W_{xh} are the weight matrices between the input x

and the reset gate, update gate, and candidate activation, respectively; W_{hr}, W_{hz}, and W_{hh} are the weight matrices between the hidden state h and the reset gate, update gate, and candidate activation, respectively; and b_r, b_z, and b_h are the corresponding bias terms. The dot symbol denotes the element-wise product.

$$\begin{aligned} r_t &= \sigma(W_{xr}x_t + W_{hr}h_{t-1} + b_r) \\ z_t &= \sigma(W_{xz}x_t + W_{hz}h_{t-1} + b_z) \\ \widetilde{h}_t &= \tanh(W_{xh}x_t + W_{hh}(r_t \cdot h_{t-1}) + b_h) \\ h_t &= (1 - z_t) \cdot h_{t-1} + z_t \cdot \widetilde{h}_t \end{aligned} \tag{13}$$

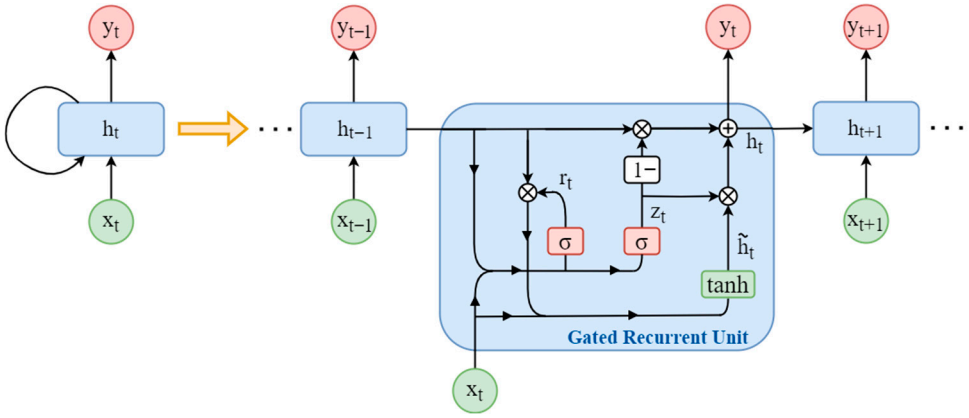

Figure 4. Graphical representation of the Gated Recurrent Unit (GRU) neural network workflow.

Finally, the output layer is represented by the linear equation in (14), where W_{hy} is the weight matrix between the hidden layer output and the network output y, and b_y is the bias term of the output layer.

$$y = W_{hy}h_t + b_y \tag{14}$$

Thanks to its internal gating mechanisms, a GRU has the additional capability of learning patterns in the input sequence and storing relevant information in memory. The gates control the flow of information, retaining important information over long sequences and discarding irrelevant data. In this way, GRUs, like LSTMs, are specifically designed to mitigate the vanishing gradient problem that affects traditional RNNs. Moreover, GRUs have a simpler structure than LSTMs, with fewer parameters to train, which can result in faster training times and reduced computational cost. However, GRUs lack an explicit output gate, which is present in LSTMs and can be beneficial for certain tasks where controlling the output flow is crucial. In the present application, an RNN was required because of the sequence-to-one regression nature of the problem; however, explicit control of the output flow is not a key requirement. For this reason, a GRU-based NN architecture has been selected for this study. The GRU architecture was selected as a compromise between modeling capability and computational complexity. Compared to LSTM networks, GRUs require fewer parameters while maintaining the ability to capture temporal dependencies, which is particularly important for real-time embedded implementation. Transformer-based architectures were also considered; however, they typically require larger datasets and higher computational resources, making them less suitable for real-time execution on embedded controllers. Since the input sequences are relatively short and the system dynamics can be effectively captured using recurrent architectures, the GRU network represents an appropriate trade-off between estimation accuracy and computational efficiency.

NNs are increasingly being applied to estimate parameters in power electronic converters. As stated in the previous chapters, traditional methods for parameter estimation often require complex mathematical modelling and analysis. However, NNs offer an alternative

approach that can handle non-linear dynamics and time-varying behaviour without the need for explicit mathematical models. This makes NNs suitable for complex and real-time applications.

In this paper, the real-time estimation of the inductances of the L-type filter of the AC–DC converter and the DC-link capacitance is carried out using a GRU-based NN. The final architecture of the NN, illustrated in Figure 5, consists of a single hidden layer composed of 64 neurons. The NN is trained on data obtained first from simulations and later from measurements of the HIL emulation of the converter. The number of hidden neurons was selected through empirical hyperparameter tuning. Networks with 16, 32, 64, and 128 neurons were tested. The configuration with 64 neurons provided the best trade-off between estimation accuracy and computational cost for real-time implementation. The training dataset was generated from Typhoon HIL simulations and consists of 41 multivariate time-series sequences, each including seven input channels (I_A, I_B, I_C, THD_{ia}, THD_{ib}, THD_{ic}, and V_{dc}). The dataset was randomly split into 32 training samples, 5 validation samples, and 4 test samples. The GRU network was trained in MATLAB using the Adam optimizer for 5000 epochs, with a mini-batch size of 32 and an initial learning rate of 0.00025. These quantities were selected because they are directly influenced by variations in the passive parameters to be estimated and are therefore highly sensitive indicators of changes in the inductances and the DC-link capacitance. In particular, the current waveforms and their harmonic content reflect the dynamic response of the AC-side filter, while the DC-link voltage profile is tightly coupled to the energy storage behavior of the capacitor. As a result, this combination of routinely measured signals provides the NN with the most informative and physically meaningful features for distinguishing different parameter conditions, without requiring additional sensors or intrusive excitation signals. Once trained, the NN is deployed online in the system, where it continuously estimates the parameters as new input data are fed into the network. To conclude, the GRU NN architecture has been implemented on the microprocessor of the control board using the LabVIEW programming language. The computational time and cost of the NN-based parameter estimation algorithm are analysed in order to demonstrate the feasibility and applicability of the proposed method.

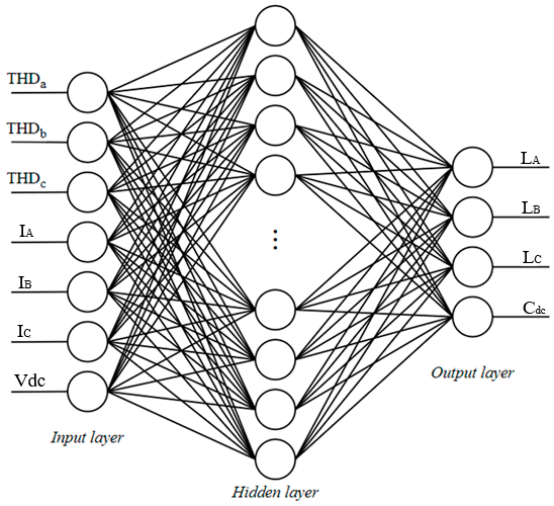

Figure 5. Proposed NN architecture.

4. Experimental Results

As previously mentioned, the training was carried out in the MATLAB environment using a dataset obtained from the AC–DC converter emulated in a Typhoon HIL 606. The inductances were randomly varied between 400 µH and 1.2 mH, and the capacitance

between 0.1 mF and 2 mF. Training, validation and testing were performed using both balanced and unbalanced inductance values in order to evaluate the estimation performance under different conditions.

The predicted values were compared with the expected ones by means of the scatter plots shown in Figure 6. In particular, the red dotted line represents the reference line where the predicted values should ideally lie in order to match the target values. The blue dots represent the parameters predicted by the NN (x-axis) versus the corresponding target values (y-axis). Figure 6a shows the inductance L_a, Figure 6b the inductance L_b, Figure 6c the inductance L_c, and in Figure 6d the capacitance C_{dc}. As can be seen, some outliers are present, meaning that the predicted value does not coincide with the expected one and therefore lies far from the red dotted line. Despite this, most of the test samples follow the reference line closely. Hence, it can be concluded that the proposed passive-parameter estimation method is promising. Table 2 reports the RMSE and MPE for each parameter.

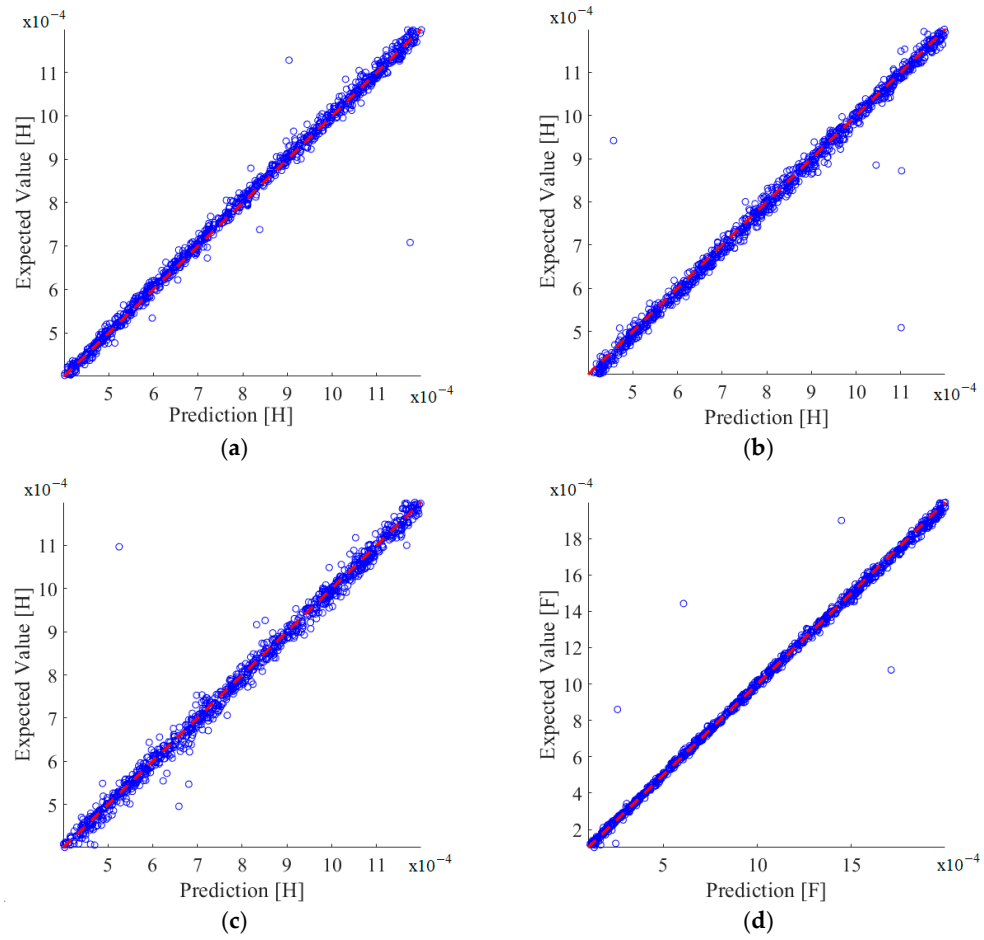

Figure 6. Predicted parameters (blue dots) compared to the expected results (red dotted line): (**a**) inductance La in the range 0.4 mH–1.2 mH; (**b**) inductance Lb in the same range; (**c**) inductance Lc in the same range; (**d**) capacitance Cdc in the range 0.1 mF–2 mF.

To further evaluate the estimation performance, additional metrics such as the mean absolute error (MAE) and the coefficient of determination (R^2) were computed, as shown in Table 2. The MAE provides the average absolute deviation between predicted and measured values, while the R^2 coefficient evaluates the goodness of fit of the model. The obtained results show very low estimation errors for all parameters. In particular, the MAE values remain on the order of 10^{-5} for all estimated quantities, while the MPE is below 1% for all inductances and below 0.1% for the DC-link capacitance. Furthermore,

the coefficient of determination is close to unity for all parameters ($R^2 \geq 0.97$), indicating excellent agreement between predicted and measured values. These results, together with the scatter plots in Figure 6, confirm that the proposed neural real-time digital twin provides highly accurate parameter estimation. The tight clustering of the data around the 1:1 reference line further demonstrates the strong correlation between predicted and measured values and the robustness of the proposed method.

Table 2. Errors in the estimation of the deterioration parameters.

Passive Parameter	RMSE	MPE	MAE	R^2
L_a	2.075×10^5	0.38%	1.62×10^5	0.98
L_b	2.950×10^5	0.97%	2.13×10^5	0.97
L_c	2.561×10^5	0.47%	1.97×10^5	0.97
C	4.442×10^5	0.077%	3.56×10^5	0.99

To further validate the proposed method for parameter identification of the boost rectifier, an experimental setup was built. Figure 7 shows the experimental test rig used to validate the proposed algorithm. From the figure, the PMSM directly coupled to the generator, the three-phase boost rectifier, the control board and the adapter board can be identified. The main parameters of the PMSM are reported in Table 3.

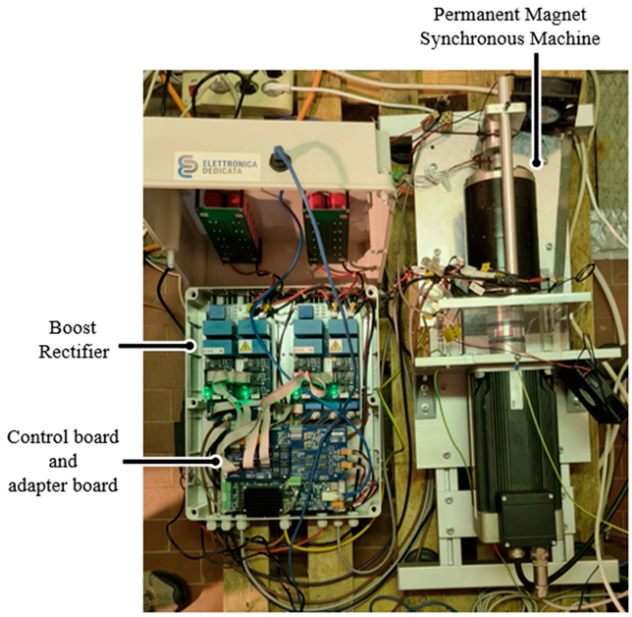

Figure 7. Experimental test rig.

The converter consists of a three-phase power stage mounted on an air-extruded heat sink. On top of each heat sink, there is a Semikron-Danfoss three-phase power module (Skiip-26ACM12V17, 1200 V, 72 A) with SiC MOSFET devices, the gate-drive circuits, three current sensors (LEM LAH50-P), one DC-side voltage sensor (LEM LV20-P), and four TDK film capacitors. The control structure, data acquisition and buffering were implemented on the FPGA of the PED-Board® controller using the LabVIEW environment. This implementation enables real-time analysis by transmitting data directly to the on-board microprocessor, where the closed-form representation of the ANN has been implemented using LabVIEW Real-Time, as illustrated in Figure 8.

Table 3. Main parameters of the PMSM.

Name of the Parameter	Value
PM machine rated phase EMF [V_{rms}]	245
Rated current [A_{rms}]	25
PM machine rated speed [rpm]	3000
Number of pair-pole	10
Magnetic flux [Wb]	0.11
PM machine inductance [μH]	420
PM machine resistance [mΩ]	550

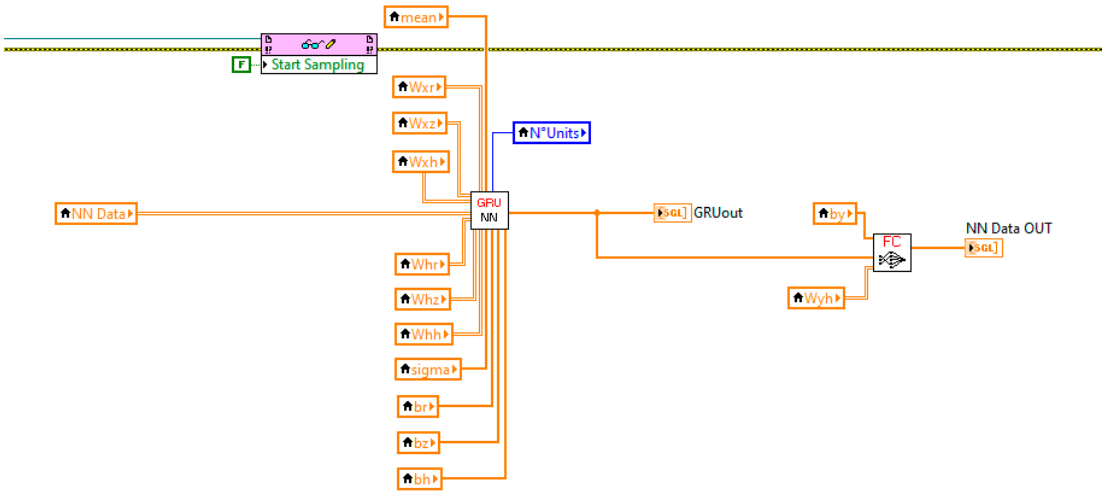

Figure 8. Development of the GRU NN in the LabVIEW Real-Time environment.

The input data are first sampled using a dedicated trigger. The sampling process is automatically stopped after two fundamental periods, and the sampled data are stored in the variable "NNData". This variable is provided as an input to the "GRU NN" subVI, together with the weights and biases obtained in MATLAB during the training process. Figure 9 shows the implementation of the closed-form equations in (14) inside the "GRU NN" subVI in LabVIEW Real-Time.

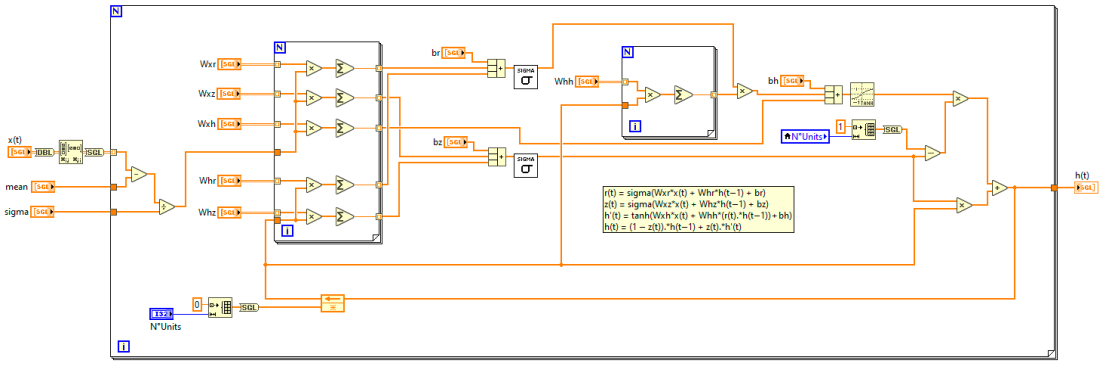

Figure 9. Internal view of the "GRU NN" subVI in the LabVIEW Real-Time environment.

As can be observed, the "GRU NN" subVI returns the updated hidden state, which is then used in the output fully connected layer implemented in the "FC" subVI to obtain the NN output value. Figure 10 shows the current waveforms I_a (yellow), I_b (green), I_c (magenta) and the DC-link voltage V_{dc} (red) at steady state when the machine speed is equal to 2500 rpm. Under these conditions, the current peak is 30 A and the peak of the electromotive force is 287 V.

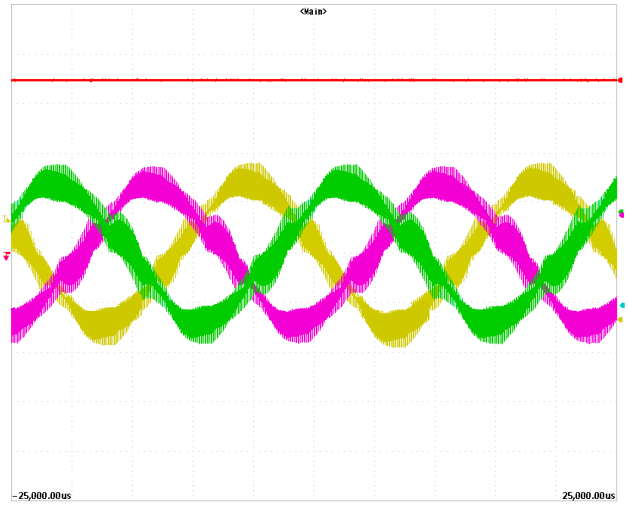

Figure 10. PMSG phase currents and DC-bus voltage: IA (yellow line), IB (green line), IC (magenta line), Vdc (red line). 20 A/div, 200 V/div, 5 ms/div.

Figure 11 shows the estimated and measured synchronous resistances, inductances and DC-bus capacitance when the temperature is close to 25 °C. As can be seen, the proposed algorithm is able to estimate the system parameters.

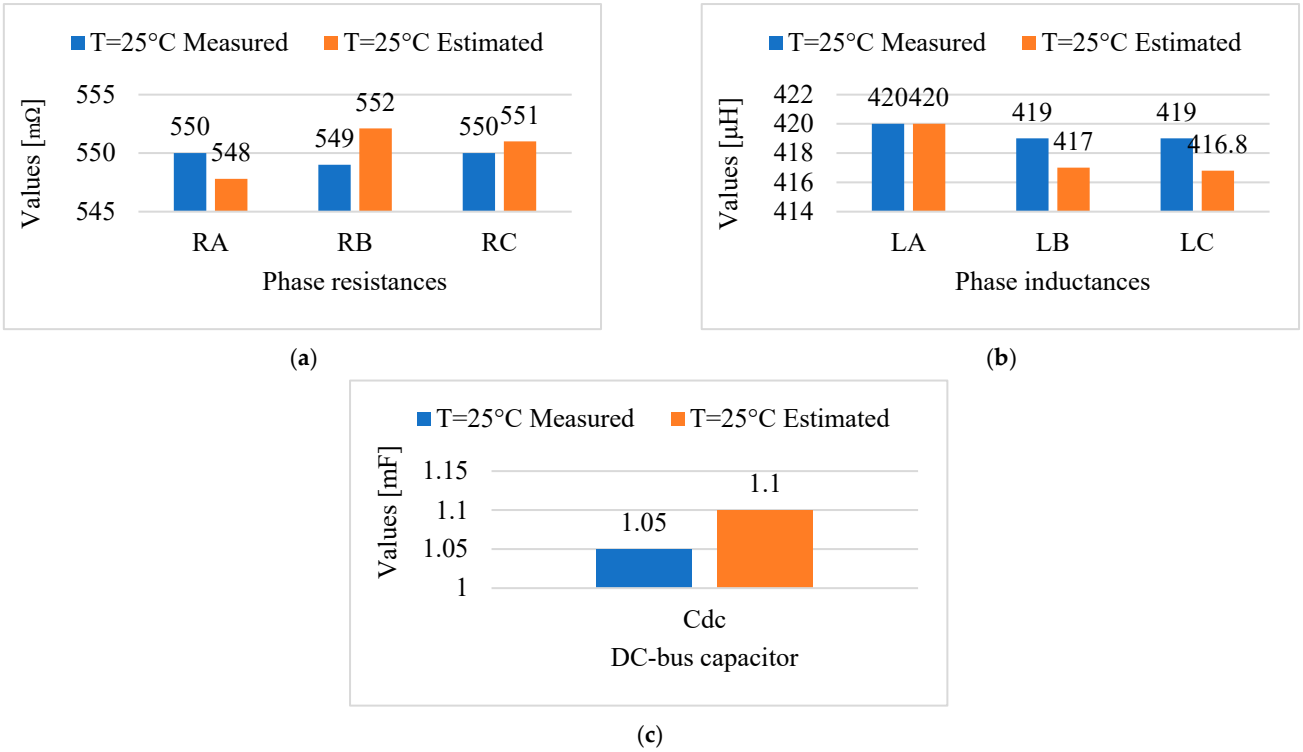

Figure 11. Measured (blue) and estimated (orange) parameters at 25 °C: (**a**) phase resistances; (**b**) phase inductances; (**c**) DC-bus capacitance Cdc.

Figure 12 illustrates the estimated and measured synchronous resistances, inductances and DC-bus capacitance when the temperature is close to 50 °C. The operating temperature was measured with a sensor placed inside the machine stator winding. An HP 4192A-LF Impedance Analyzer was used to characterize the stator windings, measuring the phase inductances without electrical load, while a multimeter was used to estimate the on-state

resistance. The inductance associated with the direct axis under operating conditions was then measured.

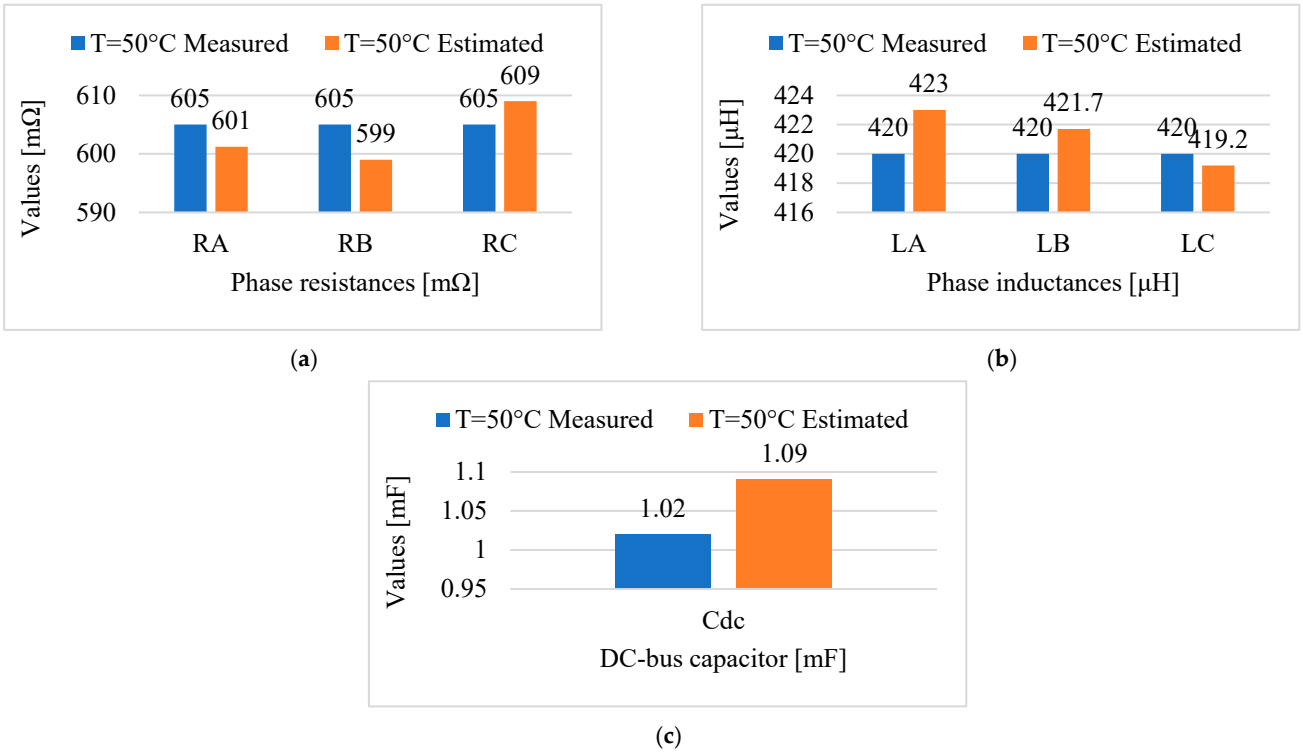

Figure 12. Measured (blue) and estimated (orange) at 50 °C: (**a**) phase resistances; (**b**) phase inductances; (**c**) DC-bus capacitance C_{dc}.

To determine this inductance, the d-axis of the rotor must be aligned with phase a of the stator winding. A simple way to achieve this alignment is through single-phase excitation, where the stator current generates a non-rotating magnetic field, whose axis coincides with the physical axis of phase a. To evaluate the inductance associated with the quadrature axis, the q-axis of the rotor must instead be aligned with the physical axis of phase a. In a three-phase system, this configuration is obtained by connecting two phases in series, resulting in a stator flux that is in quadrature (90°) with respect to the physical a-axis.

The test was performed by first aligning the rotor with one or more phases, depending on whether the direct or quadrature inductance was to be measured, and then supplying them with a voltage whose frequency and RMS value were controlled via a modulation coefficient using an inverter. By employing a current probe and an oscilloscope, the current waveform was recorded. Finally, the impedance of the excited phase was evaluated by relating the phase excitation voltage to the RMS current value. The resistance of each phase was determined using the volt–ampere method: by measuring the current flowing through the stator winding and the voltage across it, the resistance was obtained using Ohm's law. Consequently, the phase inductance was estimated as the difference between the measured impedance and the measured resistance.

To better assess the performance of the proposed neural real-time digital twin, the estimation accuracy was evaluated over a wide parameter variation range. To this end, additional inductors of 380 µH and 760 µH were connected in series with each phase of the machine. Moreover, additional capacitors of 1 µF and 2 µF were inserted into the DC-link. These modifications allowed testing the estimator under significant parameter variations representative of component aging and degradation. Figure 13 shows the measured and estimated phase resistances, inductances, and DC-link capacitance at 50 °C

for two different operating conditions: (a) $L_A = L_B = L_C = 800$ µH and $C_{dc} = 2$ µF, and (b) $L_A = L_B = L_C = 1180$ µH and $C_{dc} = 3$ µF. As can be observed, the estimated parameters closely follow the measured values in both cases, confirming the capability of the proposed neural digital twin to track large parameter variations. The estimation error remains very small across all parameters. For the phase resistances, the maximum deviation is below 1%, while for the inductances the error remains below 0.8%. The DC-link capacitance estimation shows an error below 0.5% even under large capacitance variation. Considering the wide variation range introduced in the experimental setup, these results confirm the high accuracy and robustness of the proposed method. These results indicate that the proposed neural digital twin remains accurate under varying operating conditions, which emulate the dynamic load behavior typical of wind energy conversion systems. To further validate the robustness of the proposed method under asymmetric operating conditions, an additional test was performed by introducing phase inductance unbalance. In this case, the installed inductances were set to $L_A = L_B = 800$ µH and $L_C = 420$ µH. The corresponding measured and estimated parameters at 50 °C are shown in Figure 14. As can be observed, the neural real-time digital twin is able to correctly estimate the different inductance values for each phase, demonstrating its capability to operate under unbalanced load conditions. The estimation accuracy remains high even in the presence of significant phase asymmetry, confirming the robustness of the proposed approach in realistic operating scenarios.

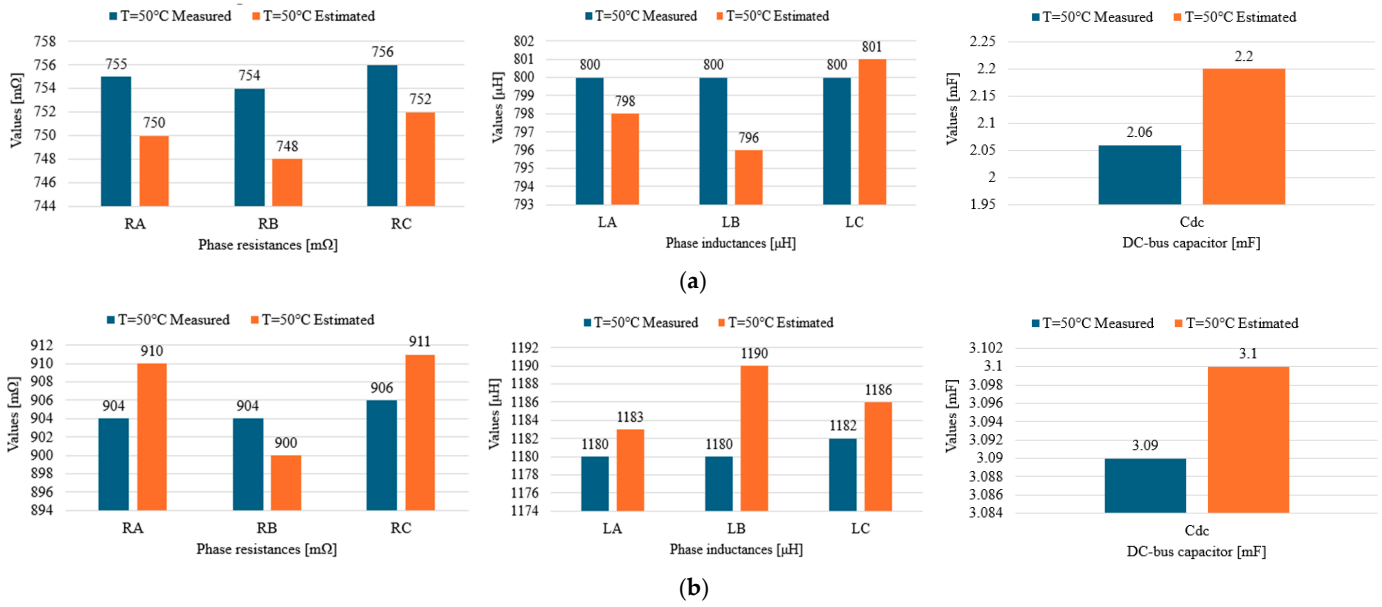

Figure 13. Measured (blue) and estimated (orange) phase resistances, inductances, and DC-link capacitance at 50 °C for two operating conditions: (**a**) $L_A = L_B L_C = 800$ µH and $C_{dc} = 2$ µF, and (**b**) $L_A = L_B L_C = 1180$ µH and $C_{dc} = 3$ µF.

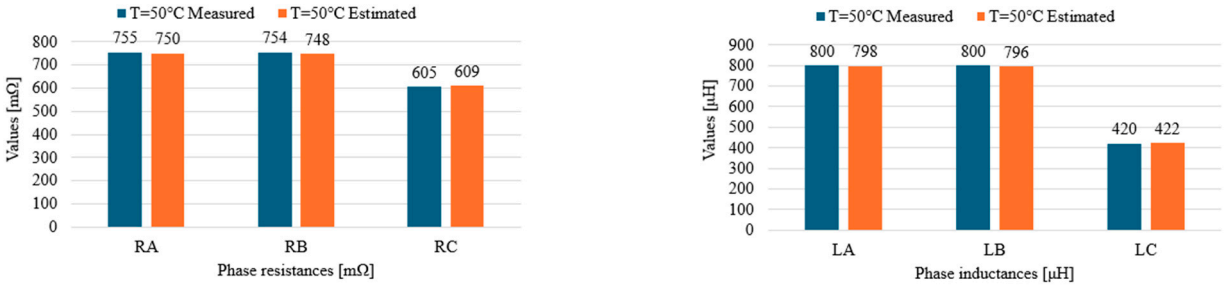

Figure 14. Measured (blue) and estimated (orange) phase resistances and inductances at 50 °C under unbalanced phase conditions: $L_A = L_B = 800$ µH, $L_C = 420$ µH.

These results also demonstrate that the neural real-time digital twin is able to correctly track parameter changes caused by hardware modifications, which emulate degradation phenomena occurring in real applications. Moreover, the estimation remains stable under temperature variations, as previously shown in Figures 11 and 12, where the estimated parameters follow the measured values with minimal deviation. Another important performance metric is the capability of the proposed method to simultaneously estimate multiple parameters. Unlike conventional NN-based estimators that focus on a single component, the proposed approach identifies stator resistance, synchronous inductance, and DC-link capacitance within a unified framework. This multi-parameter estimation capability is particularly relevant for condition monitoring applications, where degradation may affect different components simultaneously. Finally, compared to state-of-the-art NN-based estimators reported in [24–30], as shown in Table 4. The proposed method provides competitive estimation accuracy while enabling real-time embedded execution and system-level monitoring. The combination of multi-parameter estimation, real-time implementation, and low estimation error highlights the effectiveness of the proposed neural real-time digital twin for condition monitoring of power conversion systems.

Table 4. Comparison with state-of-the-art NN-based parameter estimation methods.

Reference	System	Estimated Parameters	Method	Real-Time	Multi-Parameter	Error
[24]	Back-to-back converter	DC-link capacitance	ANN	No	No	~2–3%
[25]	Buck converter	Converter parameters	BP-ANN	No	Yes	~2%
[27]	Boost converter	Degradation parameters	NN	Partial	No	~1–2%
[29]	Induction motor	R_s, R_r	ANN	Yes	No	~1%
Proposed	PMSG + rectifier	R_s, L_s, C_{dc}	GRU DT	Yes	Yes	<1%

5. Conclusions

This paper has presented an enhanced neural real-time digital twin for a PMSG-based power conversion system intended for offshore wind applications. The DT is built around a GRU neural network that estimates in real time the PMSG phase resistance and synchronous inductance, as well as the DC-link capacitance of a three-phase boost rectifier. Unlike traditional model-based identification techniques, the proposed approach leverages only routinely measured electrical quantities and does not require additional sensors or intrusive test procedures. The GRU network was first trained and validated using a Typhoon HIL 606 emulator of the AC–DC conversion stage, where the inductances and capacitance were randomly varied over wide ranges and both balanced and unbalanced conditions were considered. Scatter-plot analysis and numerical indicators (RMSE and MPE) showed that the predicted parameters closely follow their reference values, with most samples lying near the ideal 1:1 line and mean percentage errors below 1% for all quantities. These results confirm the capability of the proposed NN-based RTDM to capture the nonlinear and time-varying behaviour of the system.

To further validate the method, an experimental test rig was developed including a PMSG, a three-phase boost rectifier with SiC devices, and a PED-Board® controller. The GRU closed-form equations were implemented on the controller using LabVIEW Real-Time, enabling embedded execution with limited computational resources. Experimental measurements at different operating temperatures (around 25 °C and 50 °C) confirmed

that the DT correctly tracks the evolution of the synchronous resistances, inductances, and DC-link capacitance, demonstrating robustness with respect to thermal variations and practical operating conditions.

Overall, the results indicate that the proposed GRU-based digital twin is an effective and computationally efficient tool for online parameter identification in power electronic converters and electrical drives. By providing accurate real-time estimates of key degradation-sensitive parameters, it lays the groundwork for advanced condition monitoring and predictive maintenance strategies in offshore wind power conversion systems. Future research will focus on extending the proposed neural real-time digital twin toward fault detection capabilities by identifying specific component degradations in the PMSG and power converter. Moreover, the integration of the digital twin with predictive maintenance strategies will be investigated, enabling the estimation of degradation trends and supporting remaining useful life prediction and maintenance scheduling in offshore wind applications.

Author Contributions: Conceptualization, M.d.B., V.R. and A.A.; methodology, M.d.B., V.R. and G.G.; software, G.G.; validation, M.d.B., L.S., A.L., V.R. and G.G.; formal analysis, M.d.B., A.L., A.A., L.S., G.C. and G.G.; investigation, M.d.B., A.L.,V.R. and G.G.; resources, M.d.B., V.R., E.G.A.P. and A.A.; data curation, M.d.B. and A.L.; writing—original draft preparation, M.d.B.; writing—review and editing, V.R., M.d.B. and A.A.; visualization, M.d.B.; supervision, M.d.B., V.R., L.S., E.G.A.P. and A.A.; project administration, M.d.B., V.R., E.G.A.P. and A.A.; funding acquisition, M.d.B., V.R., E.G.A.P. and A.A. All authors have read and agreed to the published version of the manuscript.

Funding: This study was carried out within the "Enhanced Neural real-time digital TWIN for Electrical Drives" project—funded by Ministero dell'Università e della Ricerca—within the PRIN 2022 program (Code: 2022WNX4H2, D.D.104—02/02/2022).

Institutional Review Board Statement: Not applicable.

Informed Consent Statement: Not applicable.

Data Availability Statement: The raw data supporting the conclusions of this article will be made available by the authors on request.

Acknowledgments: The authors would like to thank Marco Salvi and E.D. Elettronica Dedicata S.r.l. for providing the full-SiC power converter, drives, adapter board, and PED-Board® used in the experimental campaign (https://www.ped-hub.com/).

Conflicts of Interest: The authors declare no conflicts of interest.

References

1. Fischer, K.; Stalin, T.; Ramberg, H.; Wenske, J.; Wetter, G.; Karlsson, R.; Thiringer, T. Field-Experience Based Root-Cause Analysis of Power-Converter Failure in Wind Turbines. *IEEE Trans. Power Electron.* **2015**, *30*, 2481–2492. [CrossRef]
2. Di Nezio, G.; Di Benedetto, M.; Ghione, G.; Randazzo, V.; Solero, L. Digital twin based identification of passive parameters of three-phase boost rectifier using a gru neural network. In Proceedings of the 2024 IEEE Energy Conversion Congress and Exposition (ECCE), Phoenix, AZ, USA, 20–24 October 2024.
3. Luo, Y.; Xiao, F.; Wang, B.; Liu, B. Failure analysis of power electronic devices and their applications under extreme conditions. *Chin. J. Electr. Eng.* **2016**, *2*, 91–100. [CrossRef]
4. Abuelnaga, A.; Narimani, M.; Bahman, A.S. Power electronic converter reliability and prognosis review focusing on power switch module failures. *J. Power Electron.* **2021**, *21*, 865–880. [CrossRef]
5. Yang, S.; Bryant, A.; Mawby, P.; Xiang, D.; Ran, L.; Tavner, P. An industry-based survey of reliability in power electronic converters. In *2009 IEEE Energy Conversion Congress and Exposition*; IEEE: New York, NY, USA, 2009; pp. 3151–3157.
6. Ni, Z.; Lyu, X.; Yadav, O.P.; Singh, B.N.; Zheng, S.; Cao, D. Overview of Real-Time Lifetime Prediction and Extension for SiC Power Converters. *IEEE Trans. Power Electron.* **2020**, *35*, 7765–7794. [CrossRef]

7. Bęczkowski, S.; Ghimre, P.; de Vega, A.R.; Munk-Nielsen, S.; Rannestad, B.; Thøgersen, P. Online Vce measurement method for wear-out monitoring of high power IGBT modules. In *Proceedings of the 2013 15th European Conference on Power Electronics and Applications (EPE), Lille, France, 3–5 September 2013*; IEEE: New York, NY, USA, 2013; pp. 1–7.
8. Smet, V.; Forest, F.; Huselstein, J.-J.; Rashed, A.; Richardeau, F. Evaluation of Vce Monitoring as a Real-Time Method to Estimate Aging of Bond Wire-IGBT Modules Stressed by Power Cycling. *IEEE Trans. Ind. Electron.* **2013**, *60*, 2760–2770. [CrossRef]
9. Mandeya, R.; Chen, C.; Pickert, V.; Naayagi, R.T.; Ji, B. Gate–Emitter Pre-threshold Voltage as a Health-Sensitive Parameter for IGBT Chip Failure Monitoring in High-Voltage Multichip IGBT Power Modules. *IEEE Trans. Power Electron.* **2019**, *34*, 9158–9169. [CrossRef]
10. Zhou, L.; Zhou, S.; Xu, M. Investigation of gate voltage oscillations in an IGBT module after partial bond wires lift-off. *Microelectron. Rel.* **2013**, *53*, 282–287. [CrossRef]
11. Dupont, L.; Avenas, Y.; Jeannin, P.-O. Comparison of junction temperature evaluations in a power IGBT module using an IR camera and three thermo-sensitive electrical parameters. In *Proceedings of the 2012 Twenty-Seventh Annual IEEE Applied Power Electronics Conference and Exposition (APEC), Orlando, FL, USA, 5–9 February 2012*; IEEE: New York, NY, USA, 2012; pp. 182–189.
12. Andrade, J.M. Electrolytic Capacitor Degradation Monitoring using an On-line Parameter Estimation Scheme involving Sliding Mode Differentiators and a Kalman Filter. In *Proceedings of the 2019 21st European Conference on Power Electronics and Applications (EPE '19 ECCE Europe), Genova, Italy, 2–5 September 2019*; IEEE: New York, NY, USA, 2019; pp. P.1–P.14.
13. Wechsler, A.; Mecrow, B.C.; Atkinson, D.J.; Bennett, J.W.; Benarous, M. Condition Monitoring of DC-Link Capacitors in Aerospace Drives. *IEEE Trans. Ind. Appl.* **2012**, *48*, 1866–1874. [CrossRef]
14. Yang, S.; Xiang, D.; Bryant, A.; Mawby, P.; Ran, L.; Tavner, P. Condition Monitoring for Device Reliability in Power Electronic Converters: A Review. *IEEE Trans. Power Electron.* **2010**, *25*, 2734–2752. [CrossRef]
15. Algreer, M.; Armstrong, M.; Giaouris, D. Active Online System Identification of Switch Mode DC–DC Power Converter Based on Efficient Recursive DCD-IIR Adaptive Filter. *IEEE Trans. Power Electron.* **2012**, *27*, 4425–4435. [CrossRef]
16. Di Nezio, G.; Marini, G.; Di Benedetto, M.; Lidozzi, A.; Solero, L. Digital Twin Based Identification of Passive Parameters for PMSM-Based Generating Unit by an Extended Kalman Filter for Wind Off-Shore Applications. In *Proceedings of the 2024 International Symposium on Power Electronics, Electrical Drives, Automation and Motion (SPEEDAM), Napoli, Italy, 19–21 June 2024*; IEEE: New York, NY, USA, 2024; pp. 1191–1196.
17. Grieves, M. Digital twin: Manufacturing excellence through virtual factory replication. *White Pap.* **2014**, *1*, 1–7.
18. Chen, S.; Wang, S.; Wen, P.; Zhao, S. Digital Twin for Degradation Parameters Identification of DC-DC Converters Based on Bayesian Optimization. In *Proceedings of the 2021 IEEE International Conference on Prognostics and Health Management (ICPHM)*; IEEE: New York, NY, USA, 2021; pp. 1–9.
19. Wunderlich, A.; Santi, E. Digital Twin Models of Power Electronic Converters Using Dynamic Neural Networks. In *Proceedings of the 2021 IEEE Applied Power Electronics Conference and Exposition (APEC)*; IEEE: New York, NY, USA, 2021; pp. 2369–2376.
20. Di Nezio, G.; De López Diz, S.; Di Benedetto, M.; Lidozzi, A.; Peña, E.J.B.; Solero, L. Parameters Estimation of a 3-Phase AC-DC Converter based on the Digital Twin Method. In *Proceedings of the 2023 IEEE Energy Conversion Congress and Exposition (ECCE), Nashville, TN, USA, 29 October–2 November 2023*; IEEE: New York, NY, USA, 2023; pp. 2937–2944.
21. Choksi, K.; Mirza, A.B.; Zhou, A.; Singh, D.; Hijikata, M.; Luo, F. Self-Evolving Digital Twin-Based Online Health Monitoring of Multiphase Boost Converters. *IEEE Trans. Power Electron.* **2023**, *38*, 16100–16117. [CrossRef]
22. Di Nezio, G.; Di Benedetto, M.; Lidozzi, A.; Solero, L. Digital-Twin Based Health Monitoring for Multi-Phase Boost Rectifier in Wind Offshore Applications. *IEEE J. Emerg. Sel. Top. Power Electron.* **2024**, *13*, 2738–2748. [CrossRef]
23. Chen, H.; Zhang, Z.; Karamanakos, P.; Rodriguez, J. Digital Twin Techniques for Power Electronics-Based Energy Conversion Systems: A Survey of Concepts, Application Scenarios, Future Challenges, and Trends. *IEEE Ind. Electron. Mag.* **2023**, *17*, 20–36. [CrossRef]
24. Soliman, H.; Wang, H.; Blaabjerg, F. Capacitance estimation for dc-link capacitors in a back-to-back converter based on Artificial Neural Network algorithm. In *Proceedings of the 2016 IEEE 8th International Power Electronics and Motion Control Conference (IPEMC-ECCE Asia), Hefei, China, 22–26 May 2016*; IEEE: New York, NY, USA, 2016; pp. 3682–3688.
25. She, Z.; Chen, G. Full-Parameter Identification of BUCK Converter Based on Time-Domain Mapping Neural Network. In *Proceedings of the 2022 IEEE International Power Electronics and Application Conference and Exposition (PEAC), Guangzhou, China, 4–7 November 2022*; IEEE: New York, NY, USA, 2022; pp. 1000–1004.
26. Lu, C.; Li, J.; Chen, K.; Zhou, W.; Wu, Q.; Ke, J. System-level Parameters Identification for DC-DC Converters Based on Artificial Neural Network Algorithm. In *Proceedings of the 2023 IEEE Energy Conversion Congress and Exposition (ECCE), Nashville, TN, USA, 29 October–2 November 2023*; IEEE: New York, NY, USA, 2023; pp. 2932–2936.
27. Lu, Y.; Zhang, M.; Nordström, L.; Xu, Q. An Online Digital Twin based Health Monitoring Method for Boost Converter using Neural Network. In *Proceedings of the 2023 IEEE Energy Conversion Congress and Exposition (ECCE), Nashville, TN, USA, 29 October–2 November 2023*; IEEE: New York, NY, USA, 2023; pp. 3701–3706.

28. Lin, B.H.; Tsai, J.T.; Lian, K.L. A Non-Invasive Method for Estimating Circuit and Control Parameters of Voltage Source Converters. *IEEE Trans. Circuits Syst. I Regul. Pap.* **2019**, *66*, 4911–4921. [CrossRef]
29. Karanayil, B.; Rahman, M.F.; Grantham, C. Online Stator and Rotor Resistance Estimation Scheme Using Artificial Neural Networks for Vector Controlled Speed Sensorless Induction Motor Drive. *IEEE Trans. Ind. Electron.* **2007**, *54*, 167–176. [CrossRef]
30. Orlowska-Kowalska, T.; Kaminski, M. FPGA Implementation of the Multilayer Neural Network for the Speed Estimation of the Two-Mass Drive System. *IEEE Trans. Ind. Inform.* **2011**, *7*, 436–445. [CrossRef]
31. Fassi, Y.; Heiries, V.; Boutet, J.; Boisseau, S. Toward Physics-Informed Machine-Learning-Based Predictive Maintenance for Power Converters—A Review. *IEEE Trans. Power Electron.* **2024**, *39*, 2692–2720. [CrossRef]
32. Ghione, G.; Macha, J.; Randazzo, V.; Di Nezio, G.; Di Benedetto, M.; Badami, M.; Pasero, E.; Faundez-Zanuy, M. Passive parameters identification of a threephase ac–dc converter via a gru network and derivative approximations. In *Neural Networks: Overview of Current Theories and Applications*; Springer: Berlin/Heidelberg, Germany, 2025.
33. Chen, S.; Zhang, J.; Wang, S.; Wen, P.; Zhao, S. Circuit Parameter Identification of Degrading DC-DC Converters Based on Physics-informed Neural Network. In *Proceedings of the 2022 Prognostics and Health Management Conference (PHM-2022 London), London, UK, 27–29 May 2022*; IEEE: New York, NY, USA, 2022; pp. 260–268.
34. Delrio, F.; Randazzo, V.; Cirrincione, G.; Pasero, E. Physics informed neural network for continuous and cuffless arterial blood pressure. In *Proceedings of the 2025 IEEE International Conference on Artificial Intelligence for Learning and Optimization (ICoAILO)*; IEEE: New York, NY, USA, 2025; pp. 143–148.